Optimal Design of Reverse Blocking IGCT for Hybrid Line Commutated Converter

Chunpin Ren, *Student Member, IEEE*, Jiapeng Liu, Xiaozhao Li, Yue Song, Lihui Xu, Zongze Wang, Biao Zhao, *Senior Member, IEEE*, Zhanqing Yu, *Member, IEEE*, Jinpeng Wu, and Rong Zeng, *Senior Member, IEEE*

***Abstract*—The hybrid line commutated converter topology has been verified to reduce the commutation failure probability effectively, but the reverse blocking integrated gate commutated thyristor (RB-IGCT) that meets the requirements of this topology has not yet been developed. This article focuses on the optimal design of the RB-IGCT with high blocking voltage, large ON-state current, and high turn-OFF capability. First, an emitter isolation structure is proposed to tune the low-level injection efficiency, and the forward leakage current can be reduced by 50% without degrading the ON-state current. Then, a method for optimizing anode emitter is presented. A high-doped and shallow p^+ emitter is preferred to control the current gain while ensuring a low ON-state voltage. As to the turn-OFF capability, the corrugated p-base structure is used to independently improve the maximum controllable current (MCC). In addition to the corrugation amplitude, the effect of the corrugation width is verified by experiments. Finally, 8 kV RB-IGCT samples are fabricated and tested, which reach over 3 kA average ON-state current and 5.5 kA MCC. This article not only provides a practical guidance to the design of the RB-IGCT, but also promotes the development of the HVdc transmission system.**

***Index Terms*—Reverse blocking integrated gate commutated thyristor (RB-IGCT), line commutated converter, thyristor.**

I. Introduction

THE conventional line-commutated converter-based high voltage direct current (LCC-HVDC) transmission system is one of the best choices for long-distance large-capacity transmission [1], but its safe and stable operation is seriously threatened by commutation failures [1], [2]. Recently, a new hybrid line commutated converter (*H-LCC*) topology based on reverse blocking integrated gate commutated thyristor (RB-IGCT) has been proposed. In *H-LCC*, a part of the thyristors is replaced by fully-controlled IGCTs, as shown in Fig. 1 [3]. The strong active turn-OFF capability and extremely small extinction angle of the RB-IGCT can reduce the probability of commutation failure and improve the economy of the transmission systems by reducing the reactive power loss.

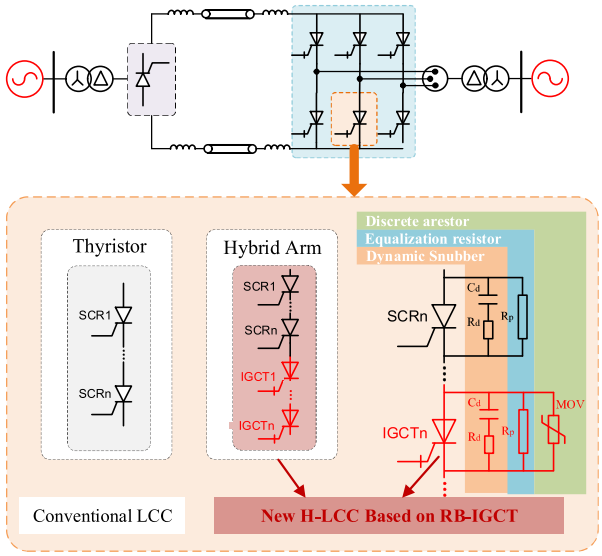

Fig. 1. Topology of conventional *LCC* and the new *H-LCC* based on RB-IGCT.

The RB-IGCT used in the proposed *H-LCC* needs to fulfill the following three conditions.

1) The bidirectional blocking voltage should be higher than 8 kV to replace the thyristors in equal amounts.
2) The average ON-state current I_{TAV} should be more than 3 kA to adapt to ultrahigh voltage (UHV) projects.
3) The device needs a strong active turn-OFF capability to overcome the commutation failure. If the maximum controllable current (MCC) is greater than 5.5 kA, more than 90% of the commutation failure can be avoided. This 90% is calculated based on the current, *di/dt*, and turn-OFF action time under extreme operating conditions of the system.

Currently, exiting RB-IGCTs cannot meet the demand of *H-LCC*. The available 2.5 kV RB-IGCT [4] is optimized for 1 kV

Manuscript received 20 December 2022; revised 12 March 2023, 8 May 2023, and 20 June 2023; accepted 22 July 2023. Date of publication 8 August 2023; date of current version 22 September 2023. This work was supported in part by the General projects of the National Natural Science Foundation under Grant 52177153, in part by the Young Scientists Found of the National Natural Science Foundation of China under Grant 52207164, and in part by the Integration projects of National Natural Science Foundation of China-State Grid Joint Fund for Smart Grid under Grant U1966602. Recommended for publication by Associate Editor C. DiMarino. *(Corresponding authors: Jinpeng Wu; Jiapeng Liu.)*

Chunpin Ren, Zongze Wang, Biao Zhao, Zhanqing Yu, Jinpeng Wu, and Rong Zeng are with the Department of Electrical Engineering, Tsinghua University, Beijing 100084, China. (e-mail: 18810903251@163.com; zzwang132@163.com; zhaobiao112904829@126.com; yzq@tsinghua.edu.cn; jinpengwu@tsinghua.edu.cn; zengrong@tsinghua.edu.cn).

Jiapeng Liu is with the Department of Energy and Power Engineering, Tsinghua University, Beijing 100084, China. (e-mail: 18811362403@163.com).

Xiaozhao Li, Yue Song, and Lihui Xu are with the Tsinghua Sichuan Energy Internet Research Institute, Chengdu 610299, China. (e-mail: lixiaozhao@tsinghua-eiri.org; songyue@tsinghua-eiri.org; xulihui@tsinghua-eiri.org).

Color versions of one or more figures in this article are available at https://doi.org/10.1109/TPEL.2023.3299457.

Digital Object Identifier 10.1109/TPEL.2023.3299457

dc circuit breaker, which means that the number of IGCTs will be more than three times the number of thyristors being replaced in *H-LCC*. In terms of economy and technical complexity, the large number of 2.5 kV devices in series is not suitable. Former researchers also develop a 6.5 kV RB-IGCT for current source converters [5], but the I_{TAV} is only 400 A, leading to an excessive number of parallel connections. Therefore, it is indispensable to customize RB-IGCT with high blocking voltage, large ON-state current, and large turn-OFF capability for *H-LCC*.

In addition to scaling the current and voltage by changing the device diameter and silicon specification, the real challenge of this new device is to optimize the conduction and switching characteristics of a nonpunch through (NPT) device while keeping the leakage current low. In detail, there are three contradictions in the design of the RB-IGCT with these three objectives.

1) *Blocking Voltage Versus ON-State Current*: The most common method to suppress the high-temperature leakage current and improve the blocking voltage is increasing the thickness of the wafer. But this increases the ON-state voltage and goes against the goal of a high I_{TAV} [6]. In the asymmetric IGCTs, the transparent anode and the anode short are commonly used to balance these competing parameters [7]. But, neither of them can be transferred to RB-IGCT due to the different vertical doping profile.
2) *ON-State Current Versus Turn-OFF Characteristics*: Extremely high injection efficiency leads to a high ON-state current but will affect the turn-OFF characteristics of RB-IGCT, such as the turn-OFF energy and the MCC [7], [8]. Compared to the transparent anode structure in the asymmetric devices, the deep and graded anode emitter of the RB-IGCT make the analysis of the ON-state voltage unique. Thus, the optimization principles in the RC and asymmetric IGCTs can hardly be adopted to RB-IGCTs.
3) *Active Turn-OFF Capability Versus Turn-ON Capability*: Regarding the single-cell optimization, a deep aluminum profile [9] and a stripe fortified structure [10] may deteriorate the turn-ON characteristics of the reverse blocking device. The CB structure is an effective method to increase MCC independently [11], which has been employed in AS-IGCT. It is believed that the fundamental principle of how the CB structure improves the MCC is similar in the RB-IGCT and AS-IGCT [12], [13], [14], [15], [16]. Considering the structural difference be-tween the two types of IGCT (e.g., the thickness of the N-base layer, the specific parameters of the CB structure need to be redesigned in the RB-IGCT.

The three conflicts are common to the design of RB-IGCT. Particularly, the problems of leakage current and ON-state current are more prominent in high-voltage devices which are greater than 6.5 kV.

This article makes efforts to independently optimize the blocking, conduction, and turn-OFF characteristics of RB-IGCT. First, to achieve a high blocking voltage, we propose a novel emitter isolation (EI) structure with a flat junction boundary, which is similar to but different from the anode short. This structure can reduce the high-temperature leakage current without affecting I_{TAV}. Then, an optimal anode doping profile is employed to tune the injection efficiency to be on the saturation boundary, which ensures a low ON-state voltage with minimal impact on the turn-OFF characteristics. Further, we introduce the CB structure in RB-IGCT. To obtain the optimal turn-OFF capability, the impact of the corrugation parameters on the MCC is scanned and analyzed in the simulation, followed by experimental verification. Finally, based on the above optimized design, customized 8 kV RB-IGCT samples are fabricated and tested. The equivalent tests of auxiliary commutation and forced commutation principle in *H-LCC* are carried out.

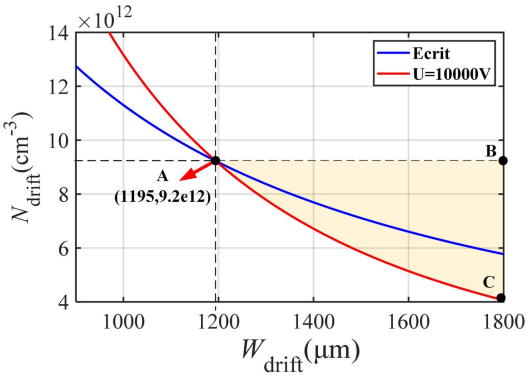

Fig. 2. Available design ranges for drift region thickness and resistivity of 8 kV RB-IGCT.

II. High-Temperature Leakage Current Control for RB-IGCT

In order to improve the blocking voltage of RB-IGCT, this article presents a detailed analysis of the leakage current control for nonpunch-through devices. The terminal of the IGCT employs a double-sided negative bevel and can help endure a high voltage from either side, which is the same as the thyristor. Thus, the design of the active region is primarily considered here. The simulations used in this article are explained in Appendix.

A. Leakage Current at High-temperature

RB-IGCT has a nonpunch-through structure with a triangular electric field distribution to achieve the bidirectional blocking capability. When the blocking voltage reaches the design value V_{set}, the peak electric field strength E_{m} cannot exceed the avalanche breakdown limit E_{C} and the width of the depletion layer cannot exceed the width of the n-drift region W_{drift}

$$E_{\mathrm{m}} = \frac{qN_{\mathrm{drift}}}{\varepsilon_{\mathrm{si}}} \times W_{\mathrm{drift}} < E_{\mathrm{C}} = 4010 \times N_{\mathrm{drift}}^{\frac{1}{8}} \quad (1)$$

$$\frac{1}{2}\frac{qN_{\mathrm{drift}}}{\varepsilon_{\mathrm{si}}} \times W_{\mathrm{drift}}^2 > V_{\mathrm{set}} \quad (2)$$

where q is the elementary charge, N_{drift} represents the doping concentration of the n-base region, and $\varepsilon_{\mathrm{si}}$ is the permittivity of silicon.

Combined with (1) and (2), the available range of the thickness and resistivity of the drift region is shown in Fig. 2. As mentioned above, the OFF-state and reverse voltage target is 8 kV, and

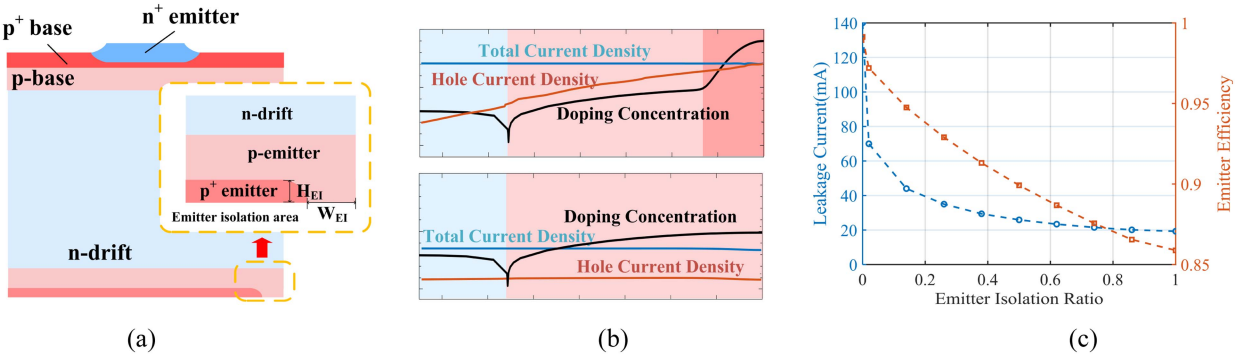

Fig. 3. (a) Structure of the EI. (b) Distribution of the total current density and hole current density of the EI structure. (c) Relationship between EI ratio, leakage current, and emitter efficiency in the forward blocking state.

the V_{set} in Fig. 2 is 10 kV with 20% margin. The blue line is the critical condition for the peak electric field, and the red line is the critical condition for the punch-through of the depletion layer. The intersection point A is the minimum thickness and corresponding resistivity to achieve the target blocking capacity. To sum up, the parameters of the drift region can be selected within the highlighted area.

In addition to the aforementioned constraints, we also need to pay attention to the high-temperature leakage current, which greatly affects the loss of the converter. With the appropriate thickness and resistivity, the high-temperature leakage current is mainly concerned with the breakdown of the open-base PNP transistors. The leakage current I_{k} in a reverse-biased junction is produced by the space-charge generation current I_{sc} and then amplified by the gain of the PNP transistor α_{pnp}

$$I_{\text{k}} = \frac{I_{\text{sc}}}{1 - \alpha_{\text{pnp}}}. \tag{3}$$

To reduce the leakage current, the width of the undepleted drift layer can be adjusted by changing the thickness of the wafer. This conventional method has limited effect. It can be demonstrated by simulations that the leakage current decreases upon thickness in a saturation trend while the ON-state voltage still increases linearly [6], [17]. Some other ideas need to be attempted.

B. Anode Emitter Isolation Structure

Here, an anode EI structure is proposed to tune the injection efficiency, as shown in Fig. 3(a). The EI structure and the anode short are both expected to independently control the emission efficiency in different injection levels. But the anode short structure used in combination with the transparent anode is not suitable for RB-IGCT. The bidirectional phase control thyristor adapts shorts on the anode side to improve the device area for both two antiparallel connected thyristors [18], [19], but the n^+ shorts on the anode side cannot tune the injection efficiency.

The anode emitter of RB-IGCT includes two layers of a low-doped deep p-emitter and a high-doped shallow p^+ emitter. The former is to cooperate with the negative bevel terminal, and the latter is to obtain the high emitter efficiency and ideal ohmic contact. In the EI structure, an anode short point is added to the

TABLE I
SATURATION ON-STATE VOLTAGE UNDER DIFFERENT PEAK CONCENTRATION OF P^+ EMITTER

N_0	$L_{\text{p+}}$	$V_{\text{sat}}(N_0, L_{\text{p+}})$
5×10^{17} cm^{-3}	75 μm	1.729 V
1×10^{18} cm^{-3}	50 μm	1.716 V
3×10^{18} cm^{-3}	35 μm	1.700 V
5×10^{18} cm^{-3}	20 μm	1.696 V
8×10^{18} cm^{-3}	15 μm	1.691 V
1×10^{19} cm^{-3}	15 μm	1.689 V

p$^+$ emitter. The anode isolation structure can divide the device into two parts in parallel, with and without a high-doped p^+ emitter, as shown in Fig. 3(b). The spatial distribution of the total and hole current density is also plotted. In the EI part, the proportion of the hole current in the p-emitter remains constant at around 0.85, while the γ_{LL} with p+ emitter is close to unity. Any γ_{LL} from 0.85 to 1 can be obtained by adjusting the anode isolation ratio.

Theoretically, the $\gamma_{LL}$is closely related to the leakage current and turn-ON characteristics, and the efficiency under high-level injection $\gamma_{HL}$is associated with the ON-state voltage. When the lateral voltage drop generated by the current flowing through the isolation region is greater than the junction voltage of the p-emitter and p$^+$ emitter, the short point of the p$^+$ emitter can be ignored. Thus, the EI structure can tune the γ_{LL} without degrading the γ_{HL}, which means that the leakage current can be reduced without affecting the I_{TAV}.

In detail, the H_{EI} depends on the thickness of the p$^+$ emitter, while the layout of the EI can adjust the W_{EI}. The quantitative effect of the isolation parameters on the device characteristics is discussed thoroughly below.

C. Impact of EI Structure on Leakage Current

Fig. 3(c) shows the relationship between the leakage current, emission efficiency, and EI ratios in the forward blocking state. The injection efficiency here refers to the ratio of the hole current density to the total current density on the J1 junction plane under low-level injection. The larger the ratio is, the

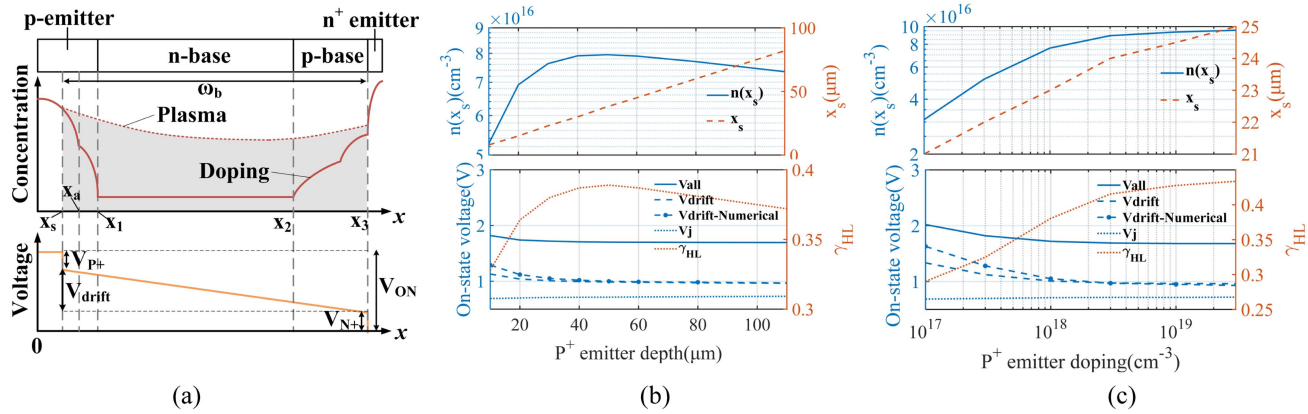

Fig. 4. (a) Plasma and the ON-state voltage distribution. (b) Relationship between L_{p+} and the internal physical parameters. (c) Relationship between N_0 and the physical parameters within the device.

smaller the emission efficiency and leakage current are, and the decreasing trend of the forward leakage current is gradually saturated. The concentration of the p^+ base region is limited by the turn-OFF capability and does not exceed 1×10^{17} cm^{-3} generally; the concentration of the p-anode is higher than that of the cathode side to optimize the ON-state voltage. Thus, the forward leakage current will be larger than the reverse leakage current. Therefore, although the EI structure has little effect on the reverse leakage current, it can reduce the maximum bidirectional leakage current.

To sum up, the EI structure with a ratio less than 0.1 can effectively reduce the forward leakage current by more than 50% without degrading the conduction characteristic.

III. Optimal Design of ON-State Current

Referring to the thyristor used in UHV *LCC* systems, RB-IGCT should have an ON-state current greater than 3 kA. In order to balance the ON-state current and turn-OFF characteristics, the anode emitter profile should be carefully designed. Here, we propose an optimized anode doping profile by simulation and explain the intrinsic mechanism. The I_{TAV} is a design target influenced by the ON-state voltage, thermal resistance, and junction temperature. As the focus is on the chip structure, the ON-state voltage becomes the key parameter in this section.

A. on-State Voltage in RB-IGCT With Graded Anode Emitter Junction

Compared to the asymmetric IGCT, the anode structure of the RB-IGCT has three unique characteristics, which make the analysis of the ON-state voltage complicated.

First, the emitter junction is a deep-graded junction, which makes the electron and hole mobilities vary upon different positions. Second, the boundary of the junction is hard to identify. When the device is turned ON, the plasma and the ON-state voltage distribution are shown in Fig. 4(a), where x_a is the boundary of the high-doped shallow junction, x_s is the boundary of the plasma region, and $n(x_s)$ is the carrier concentration at x_s. Both x_s and $n(x_s)$ change upon the current density and doping profile, which will affect the ON-state voltage. Third, the junction at x_s can be regarded as a high-low junction. The substrate doping on both sides of boundary x_s is p-type. Compared with the p-n junction, the analysis of the injection efficiency and the space charge region is different in the high-low junction.

According to the above analysis, the plasma boundary locates within the p^+ emitter region, which means, only part of the p^+ emitter acts as a real emitter (i.e., from 0 to x_s), as the other part of the p^+ emitter is in the high-level injection state (i.e., from x_s to x_1). Thus, it is mainly the highly doped part of the p^+ emitter that affects the ON-state voltage. The Gaussian doping profile of the p^+ emitter is determined by the peak doping concentration N_0 and junction depth L_{p+}. In the simulation, the ON-state voltage decreases upon N_0 and L_{p+}, and approaches to a saturation value $V_{\text{sat}}(N_0,\ L_{p+})$. If L_{p+} increases by 5 μm, the ON-state voltage decreases by no more than 0.1%, the ON-state voltage is deemed as saturated. As shown in Table I, higher N_0 makes $V_{\text{sat}}(N_0,\ L_{p+})$ smaller and the corresponding L_{p+} shallower as well. According to the above results, the N_0 of the ideal anode emitter should be greater than 5×10^{18} cm^{-3} and the L_{p+} is about 15–20 μm.

By now, the optimal design of the P^+ emitter has been achieved by the simulation. In the following part, we will illuminate intrinsically how the structural parameter L_{p+} and N_0, respectively, affect the ON-state voltage in the graded anode emitter junction.

B. on-State Voltage and the Depth of P^+ Emitter

The effect of the L_{p+} on the internal physical parameters x_s, $n(x_s)$, and high-level injection efficiency γ_{HL} is shown in Fig. 4(b); the default current density J_T is 40 A/cm^2, and the N_0 remains unchanged at 1×10^{18} cm^{-3}. The junction voltage V_j includes the V_{P+} and V_{N+}. Because the carrier concentration at x_3 hardly changes with the doping of the anode side, the change of V_j mainly related to the V_{P+}. Although the V_j slightly increases, the overall ON-state voltage is still monotonically decreasing, and the voltage drop in the drift region V_{drift} is the main factor affecting the V_{on} of the device.

It can be noted that the variation of $n(x_s)$ in Fig. 4(b) is not monotonic. When the L_{p+} is less than 50 μm, x_s increases

linearly upon the depth of the p^+ emitter, and $n(x_s)$ gradually increases and tends to saturate. Both the smaller plasma width and higher plasma concentration result in stronger conductance modulation, leading to a lower V_{drift}. When the L_{p+} is greater than 50 μm, the $n(x_s)$ begins to decease upon the L_{p+}. The reduction in the thickness of the plasma region still results in a monotonically decreasing V_{drift}, but the saturation effect makes the change only too small to be negligible. Therefore, the depth corresponding to the extreme value of $n(x_s)$ can be regarded as the saturation depth at this N_0.

With the L_{p+} increasing, both x_s and $n(x_s)$ change. The question is which one is the main factor? To decouple the effects of x_s and $n(x_s)$ on the V_{drift}, a numerical solution for the V_{drift} can used. Assuming emitter efficiency of n^+ emitter is unity and the plasma concentration at x_3 is constant, V_{drift} can be presented by x_s and $n(x_s)$ as

$$V_{drift} = \frac{kT}{2q}\ln\left(\frac{n_l}{n_r}\right) + \frac{\arctan\left(e^{\frac{\omega_B}{L_A}}\sqrt{\frac{Y}{X}}\right) - \arctan\left(\sqrt{\frac{Y}{X}}\right)}{\sqrt{XY}} \times \frac{2J_T L_A \sinh\left(\frac{\omega_B}{L_A}\right)}{q(\mu_p+\mu_n)} \quad (4)$$

$$X = n_l \sinh\left(\frac{\omega_B}{L_A}\right) + n_l \cosh\left(\frac{\omega_B}{L_A}\right) - n_r \quad (5)$$

$$Y = n_l \sinh\left(\frac{\omega_B}{L_A}\right) - n_l \cosh\left(\frac{\omega_B}{L_A}\right) + n_r \quad (6)$$

$$\omega_B = x_3 - x_s \quad (7)$$

where μ_n and μ_p represent the mobility of electrons and holes, respectively, L_A represents the ambipolar diffusion length, k represents the Boltzmann constant, and T represents the temperature.The numerical results of the V_{drift} are also shown in Fig. 4(b) for comparison with the simulated results. The mobility of the plasma region is assumed to be constant in (4), while the actual mobility between x_s and x_1 varies with doping. When L_{p+} is smaller, the proportion of the anode emission region in the plasma region is larger, resulting in the difference between the numerical calculation and the simulation results. But in the semi-quantitative decoupled analysis for x_s and $n(x_s)$, the error is acceptable.

When L_{p+} increases from 10 to 50 μm, V_{drift} decreases by 0.29 V, $n(x_s)$ increases from 5.3×10^{16} cm^{-3} to 7.9×10^{16} cm^{-3}, and x_s increases from 8 to 45 μm. According to (4), the change of $n(x_s)$ reduces V_{drift} by 0.23 V while keeping x_s unchanged, and the change of x_s reduces V_{drift} by 0.06 V while keeping $n(x_s)$ unchanged; the former accounted for 88%, while the latter for only 12%

In conclusion, the change of $n(x_s)$ has a greater effect on the V_{drift} than the effect of x_s when L_{p+} changes. The variation of $n(x_s)$ is not monotonic, and V_{drift} tends to be saturated after $n(x_s)$ reaches the maximum value. Further increasing in L_{p+} will only increase the extra diffusion time and deteriorate the turn-OFF characteristics. Therefore, in order to obtain an optimal ON-state voltage, L_{p+} should be selected before $n(x_s)$ reaches the maximum value.

C. On-State Voltage and the Peak Concentration of P^+ Emitter

The effect of N_0 on the physical parameters within the device is shown in Fig. 4(c); L_{p+} remains unchanged at 30 μm. Although x_s increases with N_0, the change is so small that the effect on V_{drift} is negligible. According to (4), the change of x_s reduces V_{drift} by 0.01V while keeping $n(x_s)$ unchanged. Thus, $n(x_s)$ can be regarded as the only variable when investigating the effect of N_0 on V_{drift}. Due to bandgap narrowing effect, when the doping concentration is particularly high, the effective doping concentration increases slightly upon N_0, and both the injection efficiency and ON-state voltage will become saturated.

In summary, an excessive injection efficiency has limited benefit to the ON-state voltage; instead, it introduces additional advance time and leads to a degradation of the turn-OFF characteristics. A p^+ emitter with a high doping and shallow layer is preferred to balance the ON-state voltage and turn-OFF characteristics. Considering the bandgap narrowing and the solid solubility of impurities, N_0 around $5\times10^{18}\sim1\times10^{19}$ cm^{-3} is acceptable; considering the nonmonotonic change of $n(x_s)$, the L_{p+} should be selected as 15–20 μm. It is noting that the analysis method is universal, which is not only applicable to the 8 kV RB-IGCT, but also to the RB-IGCT with other rated voltages.

IV. Optimal Design of Turn-OFF Capability

The novelty of the *H-LCC* topology lies in applying IGCTs' active turn-OFF characteristic to overcome commutation failures; IGCTs with larger turn-OFF current capability can cover more fault conditions. The corrugated p-base (CB) structure can effectively improve the turn-OFF capability without affecting other parameters such as turn-ON characteristic and turn-OFF loss. In this section, we first analyze the relationship between the corrugation parameters and the turn-OFF capability qualitatively through simulation, and then achieve the optimal CB structure quantitively by experiments.

A. Impact of Corrugation Parameters on MCC

The failure modes of RB-IGCT can be divided into the cathode retrigger failure and the dynamic avalanche failure; the former usually occurs at low dc-link voltages, while the latter occurs at high dc-link voltages [20]. In *H-LCC*, the overvoltage across the IGCT is usually limited by a nonlinear resistance, whose residual voltage is greater than 6 kV. Therefore, the dominating failure mode of the 8 kV RB-IGCT for *H-LCC* is the dynamic avalanche failure.

By tuning the dynamic avalanche through current redistribution, the CB structure effectively improves the dynamic avalanche limit, and eventually enhances the turn-OFF capability. During the turn-OFF process, the lateral electric field in the high-low transition redistributes the current density; the peak value of the electric field occurs under the gate contact, and the carriers generated by the dynamic avalanche can be quickly extracted from the gate. The geometry of the CB structure directly affects the modulation effect. Therefore, it is necessary to investigate the geometrical structure of the CB in the RB-IGCT.

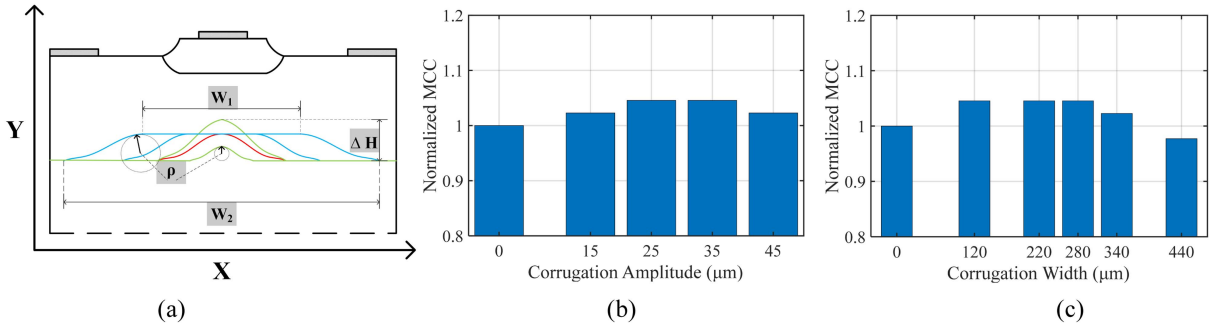

Fig. 5. (a) CB structure parameters. (b) Impact of corrugation amplitude on the normalized MCC. (c) Impact of corrugation width on the normalized MCC.

The p-base junction of different shapes is shown in Fig. 5(a). These structural features can be extracted as two key parameters—corrugation amplitude and width. The corrugation amplitude is determined by the duration and sequence of high-temperature diffusion and influences the ΔH and ρ; the corrugation width is determined by the masking width and the lateral diffusion coefficient and influences the W_1 and W_2. In order to investigate the influence of the geometrical parameters on the MCC, a two-dimensional dual-cell model is established. Gradually increasing the turn-OFF current without changing the dc-link voltage; the MCC is the maximum current derived from the last-pass waveform.

Fig. 5(b) shows the effect of corrugation amplitude on the MCC in the simulation; it has been revealed that an optimum value exists. On the one hand, if the amplitude is too large, the electric field cannot be established uniformly, making a more significant peak of the electric field appears in the high-low transfer area; on the other hand, if the amplitude is too small, a weakened horizontal electric field decreases the modulation effect of the electric field on the current density.

The effect of the corrugation width on the MCC is also not monotonic, as shown in Fig. 5(c). While the corrugation width is small, the x-component of the electric field E_x shrinks, and the current under the cathode cannot be effectively transferred to the area beneath the gate; with the corrugation width enlarging, the peak value of the E_x locates closer to the gate, and the current density right below the cathode is still large.

In summary, when the corrugation amplitude is sufficient, the closer the high-low transition area is to the center of the cathode, the better the optimization effect of the MCC will be.

B. Optimal CB Structure by Experimentation

Considering the nonquantitative results of the turn-OFF capability in the simulation, the optimal design needs to be obtained through experiments. Five different corrugation widths are set in the experiment by adjusting the masking width at equal intervals. The default corrugation depth is 25 μm. A 91 mm chip is selected instead of the targeted six-inch device for the cost consideration.

The corrugation width of sample A is the smallest, and the width of sample E is the largest. Fig. 6 shows the EBIC test results for three of the samples. The J2 junction of sample E has an apparent plateau, corresponding to the corrugation width of 340 μm in the simulation. In contrast, the high-low transition area of sample A is wholly located below the cathode

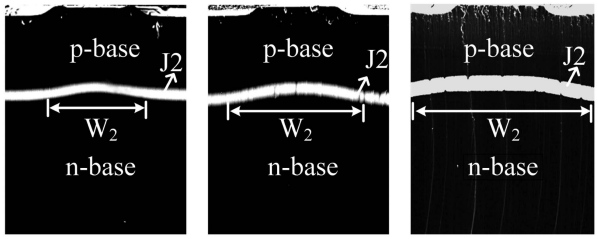

Fig. 6. EBIC test results of (a) sample A, (b) sample C, and (c) sample E.

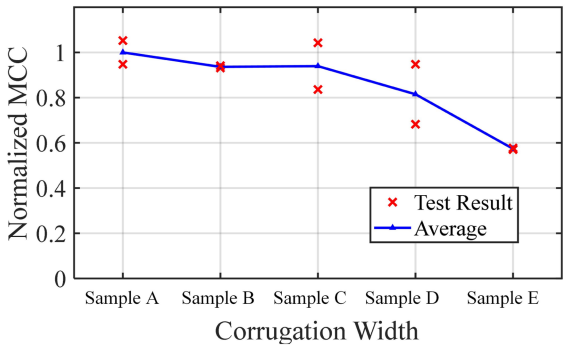

Fig. 7. MCC test results for different samples at 90 °C.

electrode, corresponding to the corrugation width of 120 μm in the simulation.

Fig. 7 shows the experimental results of the MCC of different groups of samples, which are consistent with the trends in the simulation. The test is performed on an IGCT double-pulse standard test platform with a dc-link voltage of 4 kV. The MCC of groups A, B, and C did not change much; the influence of the CB structure was smaller than the individual discrepancy. When the corrugation width is larger than sample C, the MCC starts to decrease significantly. When the corrugation width is increased to 340 μm, the MCC decreased by only 5% in the simulation but decreased by 40% in the experiment; this is mainly related to the double cell area ratio setting in the simulation.

In conclusion, the MCC will decrease significantly when the corrugation width is larger than that shown in Fig. 6(b) or larger than 300 μm. Therefore, the optimum width of the corrugation is proposed here, i.e., between 120 and 220 μm, and the results are similar to the previous work done in the AS-IGCT.

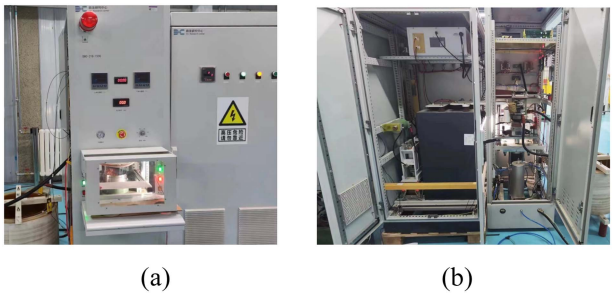

Fig. 8. Front (a) and back (b) of the test platform.

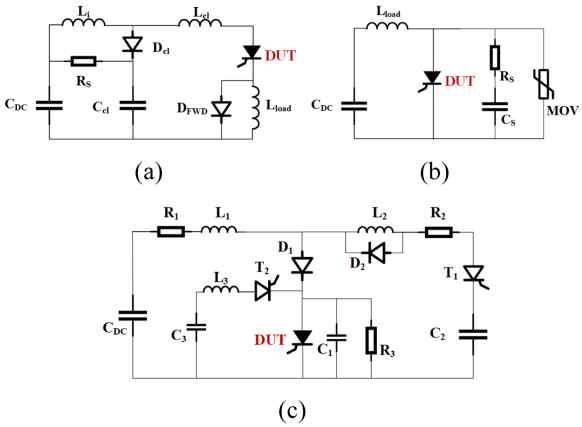

Fig. 9. The test topology for RB-IGCT. (a) Standard turn-OFF test. (b) Turn-OFF test under the forced commutation condition. (c) Circuit-commutated turn-OFF time test.

V. Experimental Verification

Based on the above analysis, 140 mm RB-IGCT samples are fabricated and irradiated to reduce the switching loss. After electron irradiation, three key parameters and the behavior in the *H-LCC* of the device are analyzed. The test platform and the topologies are shown in Figs. 8 and 9. In the test of key parameters, the comparison of the simulation results of the control group is also given. The drift region of the control group is designed as the intersection point A in Fig. 2, and the fabricated one has a thickness margin of 80 μm. The anode emitter doping profile of the control group is symmetrical with the cathode side and has no EI structure. The lifetime control in the simulation is consistent with the fabricated samples.

A. Tests on Three Key Parameters

The forward and reverse blocking characteristics are shown in Fig. 10(a). The forward leakage current $I_{\mathrm{DRM}}$and reverse leakage current I_{RRM} of the fabricated 8 kV RB-IGCT are around 50 mA when the anode voltage is 8 kV. In the simulation, the leakage current of the optimized structure is consistent with the experiment results; the control group with the same lifetime control has a larger leakage current, especially the I_{DRM}. Fig. 10(b) shows the conduction characteristics of the devices. According to the junction-to-case thermal resistance $R_{\mathrm{th}\ j-c}$ of 4.08 K/kW and the case temperature of 50 °C, and the average

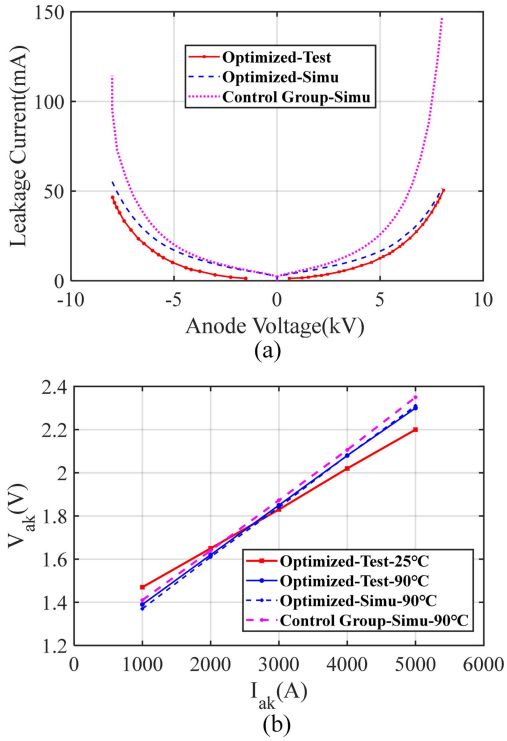

Fig. 10. (a) Blocking characteristic at 90 °C and (b) ON-state voltage of the fabricated 8kV RB-IGCT.

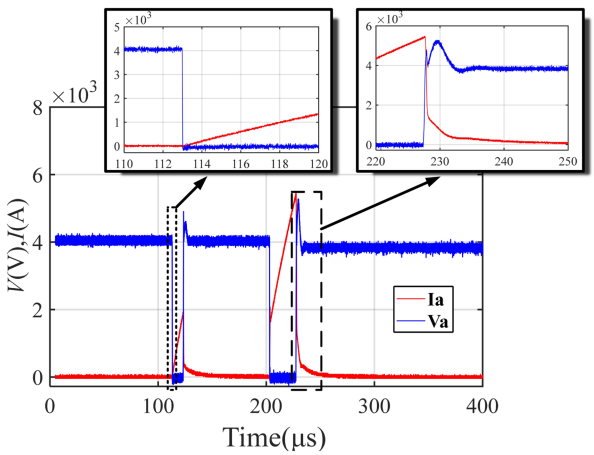

Fig. 11. Turn-OFF characteristic under 4 kV DC-link voltage in a standard double-pulse test platform at 90 °C.

ON-state current can be calculated; the ON-state voltage shown in Fig. 10(b) lead to a I_{AV} of 3200 A, which meets the requirements of the UHV project. Combined with the simulation results, the leakage current of the optimized device can be reduced by 60% with no increase in the ON-state voltage. Fig. 11 shows the test results of the device in a standard double-pulse test circuit, as well as a zoomed view of the turn-ON and turn-OFF process. The device successfully turns OFF 5.5 kA under the 4 kV. The dc-link voltage of double-pulse test is limited by the test platform, and a more critical dynamic test will be presented in Section V-B.

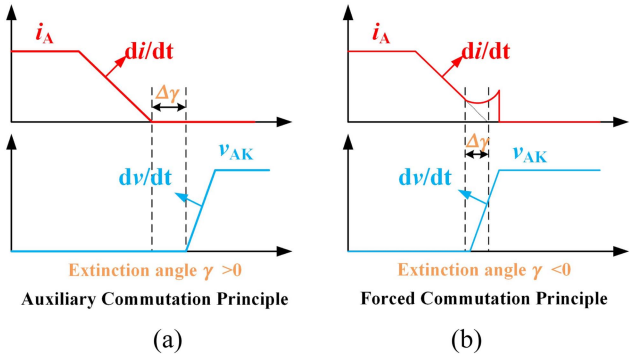

Fig. 12. Current and voltage waveforms of IGCT under different commutation principle.

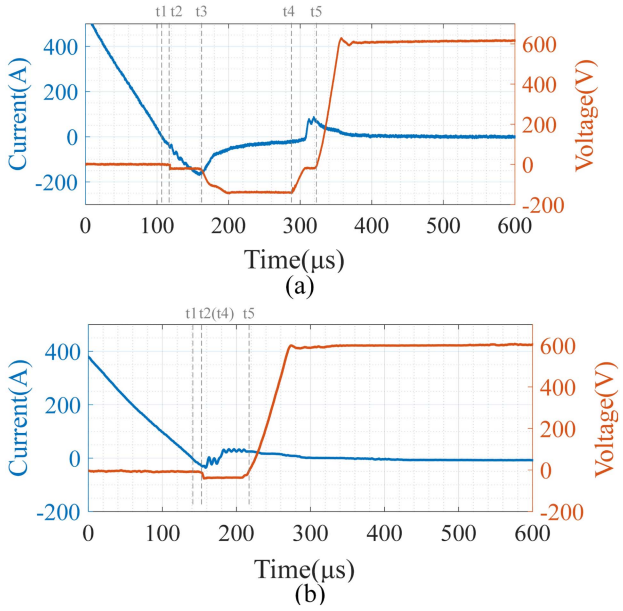

Fig. 13. Test waveform of the circuit-commutated turn-OFF time under (a) normal state and (b) critical state at 90 °C.

Thus, this fabricated device is named 8 kV/5.5 kA/3 kA RB-IGCT, representing that the blocking capability is 8 kV, the turn-OFF capability is 5.5 kA, and the ON-state current is 3 kA.

B. Behavior in H-LCC

In the application of *H-LCC*, in addition to the above parameters, we also need to pay attention to the auxiliary commutation and forced commutation, which play an important role in reducing the probability of commutation failure [3].

Under the principle of auxiliary commutation, the device begins to withstand a positive voltage after the current zero-crossing point. The interval time between the current and voltage zero-crossing is called extinction angle $\Delta\gamma$, as shown in Fig. 12(a). Commutation failure will occur if the recovery time of the device is shorter than $\Delta\gamma$. Under the principle of forced commutation, the forward *dv/dt* appears earlier than the current zero-crossing point, as shown in Fig. 12(b). When $\Delta\gamma$ is negative, the device is required to actively turn OFF and break the fault

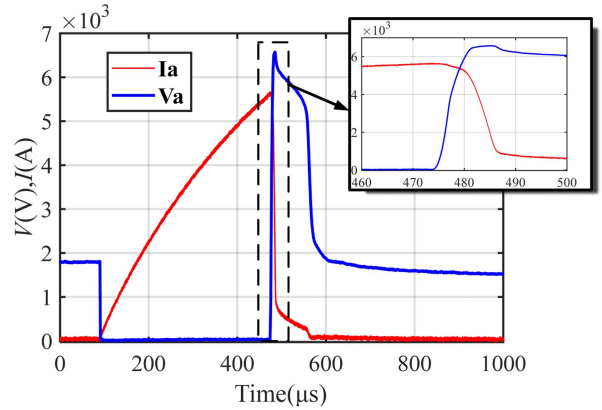

Fig. 14. Turn-OFF characteristic with a snubber *RC* and a paralleled nonlinear resistor at 90 °C.

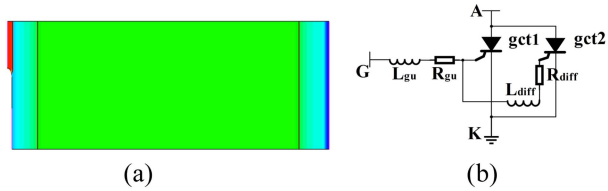

Fig. 15. (a) Half cell model. (b) Dual cell circuit topology in TCAD.

current when the current of the bridge arm which is scheduled to be turned-OFF increases abnormally.

The core indicator of the device is the circuit-commutated turn-OFF time t_q under the auxiliary commutation principle, corresponding to the extinction angle in the application. Fig. 13(a) is a typical circuit-commutated turn-OFF waveform, and the test topology is shown in Fig. 9(c). The current crosses zero at t1, and a negative voltage is applied to the gate-cathode junction at t2; the time interval between t1 and t2 is the response time of the gate drive. The J1 junction begins to establish a depletion layer and withstand negative voltage at t3, the external circuit begins to apply forward *dv/dt* at t4, and the voltage crosses zero at t5. The time interval between t1 and t5 is the circuit-commutated turn-OFF time t_q, and the time interval between t1 and t4 is called distinction time.

The t_q of the phase control thyristor used in conventional *LCC* is greater than 400 μs, while the t_q of the RB-IGCT is much smaller. Fig. 13(b) is the critical state of the circuit-commutated turn-OFF. The forward *dv/dt* is applied immediately after the gate-cathode junction is reverse-biased at t2. Because the distinction time is shorter than 20 μs, the depletion layer of the J1 junction has not started to build up before t4. Such small distinction time indicates that the RB-IGCT can withstand the forward *dv/dt* 20 μs after the current crossed zero, which achieved a significant improvement over thyristor. It should be noted that the 20 μs here is not the limit of the device itself but is limited by the detection speed of the gate drive.

The core indicator under the forced commutation condition is the maximum turn-OFF current of the device. The fabricated RB-IGCT successfully turned OFF 5.5 kA, and the peak value of the overvoltage reached 6.5 kV, as shown in Fig. 14. The test

circuit in *H-LCC* is different from the standard double pulse test platform; a snubber *RC* and nonlinear resistor are connected in parallel across the device, as shown in Fig. 9(b). Due to the small paralleled capacitor and the high residual voltage of the nonlinear resistor, the device will withstand an overvoltage greater than 5 kV for several hundred μs, which indicates that the turn-OFF process here is more severe than that under the standard double pulse test platform.

VI. Conclusion

Aiming to solve the commutation failure problem in traditional HVdc transmission projects, this article focuses on the optimal design of the RB-IGCT with high blocking voltage, high average ON-state current, and large turn-OFF capability. Through an optimization strategy of decoupling the three primary parameters, RB-IGCT samples with 8 kV/5.5 kA/3 kA are fabricated.

For the blocking voltage, an EI structure with an isolation ratio smaller than 0.1 can effectively reduce the forward leakage current by more than 50% without affecting the ON-state voltage. For the ON-state current, a P^+ emitter with N_0 around $5 \times 10^{18} \sim 1 \times 10^{19}$ cm^{-3} and L_{p+} around 15–20 μm can control the sum of the current amplification factors while ensuring a low ON-state voltage. For the turn-OFF capability, the influence of the corrugation width and amplitude on MCC is quantitatively analyzed by simulations and experiments. The results indicate that the corrugation amplitude should be between 25–35 μm and the corrugation width should be between 120–220 μm.

Practically, the RB-IGCT is employed to replace thyristors in equal quantities in the UHV *H-LCC* application, via which, the commutation failure is greatly mitigated due to the auxiliary commutation principle and forced commutation principle. In detail, by auxiliary commutation principle, RB-IGCT reduces the circuit-commutated turn-OFF time from more than 400 to 80 μs, and the critical distinction time is only 20 μs, which shows a significant improvement compared with thyristors. By forced commutation principle, the device successfully turns OFF 5.5 kA when the residual voltage of the arrester is 6.5 kV and can avoid more than 90% of the commutation failure.

We believe that this article not only proposes an optimal design of RB-IGCT with high voltage and large capacity, but also paves a feasible way to boost the revolution of the traditional *LCC* transmission system.

Appendix

A. Method of IGCT Modeling

A TCAD tool is used to investigate the impact of the design structure on the device characteristics, such as the blocking, ON-state voltage, and turn-OFF capability.

When conducting blocking and turn-ON simulations, we use a single half-cell model, as shown in Fig. 15(a). The test circuit is consistent with the test platform, and the cell area is set to match the real layout. When conducting turn-OFF simulations, gradually increasing the turn-OFF current without changing the dc-link voltage and other parameters; the maximum turn-OFF current derived from the last-pass waveform can be regarded as the MCC of this structure under certain conditions. A dual cell circuit topology is adopted, which makes a compromise between the accuracy and time-consuming [21]. The circuit topology used in the simulation is shown in Fig. 15(b). The default area ratio of gct1 and gct2 is 83:17, representing the bulk and outermost regions. The gate stray impedance of gct2 is larger than that of gct1 because the outermost region is farther away from the gate ring.

References

[1] C. V. Thio, J. B. Davies, and K. L. Kent, "Commutation failures in HVDC transmission systems," *IEEE Trans. Power Del.*, vol. 11, no. 2, pp. 946–957, Apr. 1996.

[2] F. Wang, T. Liu, and X. Li, "Decreasing the frequency of HVDC commutation failures caused by harmonics," *IET Power Electron.*, vol. 10, no. 2, pp. 215–221, 2017.

[3] C. Xu et al., "A novel hybrid line commutated converter based on IGCT to mitigate commutation failure for high-power HVDC application," *IEEE Trans. Power Electron.*, vol. 37, no. 5, pp. 4931–4936, May 2022.

[4] M. Arnold, A. Antoniazzi, M. Rahimo, D. Pessina, and U. Vemulapati, "Reverse blocking IGCT optimised for 1 kV DC bi-directional solid state circuit breaker," *IET Power Electron.*, vol. 8, no. 12, pp. 2308–2314, 2015.

[5] K. Satoh, M. Yamamoto, K. Morishita, Y. Yamaguchi, and H. Iwamoto, "High power symmetrical GCT for current source inverter," in *Proc. IEEE Int. Conf. Power Electron. Drive Syst.*, 1999, pp. 877–882.

[6] J. Vobecky, V. Botan, K. stiegler, U. Meier, and M. Bellini, "A novel ultra-low loss four inch thyristor for UHVDC," in *Proc. IEEE Int. Symp. Power Semicond. Devices ICs*, 2015, pp. 413–416.

[7] S. Bernet, E. Carroll, P. Streit, O. Steimer, P. Steimer, and S. Tschirley, "Design, test and characteristics of 10 kV IGCTs," in *Proc. IEEE Ind. Appl. Conf.*, 2003, pp. 1012–1019.

[8] S. Eicher, F. Bauer, A. Weber, H. R. Zeller, and W. Fichtner, "Punchthrough type GTO with buffer layer and homogeneous low efficiency anode structure," in *Proc. IEEE Int. Symp. Power Semicond. Devices ICs*, 1996, pp. 261–264.

[9] P. K. Steimer, H. E. Gruning, J. Werninger, E. Carroll, S. Klaka, and S. Linder, "IGCT-a new emerging technology for high power, low cost inverters," in *Proc. IEEE Ind. Appl. Conf.*, 1997, pp. 1592–1599.

[10] N. Lophitis et al., "The stripe fortified GCT: A new GCT design for max-imizing the controllable current," in *Proc. IEEE Int. Symp. Power Semicond. Devices ICs*, 2014, pp. 123–126.

[11] T. Wikstrom, T. Stiasny, M. Rahimo, D. Cottet, and P. Streit, "The corrugated p-base IGCT—A new benchmark for large area SQA scaling," in *Proc. IEEE Int. Symp. Power Semicond. Devices ICs*, 2007, pp. 29–32.

[12] F. Agostini et al., "1MW bi-directional DC solid state circuit breaker based on air cooled reverse blocking-IGCT," in *Proc. IEEE Elect. Ship Technol. Symp.*, 2015, pp. 287–292.

[13] N. Lophitis et al., "Gate commutated thyristor with voltage independent maximum controllable current," *IEEE Trans. Electron Devices Lett.*, vol. 34, no. 8, pp. 954–956, Jun. 2013.

[14] M. Arnold, T. Wikstroem, Y. Otani, and T. Stiasny, "High-temperature operation of HPT-IGCTs," in *Proc. PCIM Eur.*, 2011, pp. 32–37.

[15] T. Stiasny, U. Vemulapati, T. Wikstrom, C. Waltisberg, and M. Rahimo, "Large area (150mm) high voltage (6.5kV) reverse conducting IGCT," in *Proc. IEEE Eur. Conf. Power Electron. Appl.*, 2017, pp. 1–8.

[16] C. Wang, Y. Jing, X. Gao, and J. Han, "A new dual-GCT structure with short transparent anode and corrugated p base region," in *Proc. IEEE Int. Future Energy Electon. Conf.*, 2015, pp. 1–4.

[17] J. Vobecky, V. Botan, K. U. Meier, K. Tugan, and M. Bellini, "Local lifetime control for enhanced ruggedness of HVDC thyristors," in *Proc. IEEE Int. Symp. Power Semicond. Devices ICs*, 2018, pp. 156–159.

[18] J. Vobecky, "The bidirectional phase control thyristor," *IEEE Trans. Electron Devices*, vol. 67, no. 7, pp. 2844–2849, Jul. 2020.

[19] J. Vobecky, U. Vemulapati, and R. Bessa-Duarte, "Bidirectional phase control thyristor (BiPCT): A new antiparallel thyristor concept," in *Proc. IEEE Int. Symp. Power Semicond. Devices ICs*, 2020, pp. 54–57.

[20] C. Ren et al., "Deciphering the effect of corrugated p-base on reverse blocking IGCT," *IEEE Trans. Electron Devices*, vol. 69, no. 9, pp. 5059–5067, Sep. 2022.

[21] N. Lophitis, M. Antoniou, F. Udrea, T. Wikstrom, and I. Nistor, "Turn-off failure mechanism in large area IGCTs," in *Proc. IEEE Int. Semicond. Conf.*, 2011, pp. 361–364.